A compact and miniaturized high resolution capacitance dilatometer for measuring thermal expansion and magnetostriction

R. Küchler, T. Bauer, M. Brando, and F. Steglich
Max Planck Institute for Chemical Physics of Solids, Nöthnitzer Str. 40, 01187 Dresden, Germany

(Received 27 July 2012; accepted 15 August 2012; published online 6 September 2012)

We describe the design, construction, calibration, and two different applications of a miniature capacitance dilatometer. The device is suitable for thermal expansion and magnetostriction measurements from 300 K down to about 25 mK, with a resolution of 0.02 Å at low temperatures. The main body of the dilatometer is fabricated from a single block of a Be-Cu alloy by electrical discharge milling. This creates an extremely compact high-resolution measuring cell. We have successfully tested and operated dilatometers of this new type with the commonly used physical property measurement system by quantum design, as well as with several other cryogenic refrigeration systems down to 25 mK and in magnetic fields up to 20 T. Here, the capacitance is measured with a commercially available capacitance bridge. Using a piezoelectric rotator from Attocube Systems, the cell can be rotated at $T = 25$ mK inside of an inner vacuum chamber of 40 mm diameter. The miniaturized design for the one-axis rotation setup allows a rotation of 360°. © *2012 American Institute of Physics*. [http://dx.doi.org/10.1063/1.4748864]

I. INTRODUCTION

Since in condensed matter the entropy S measures all degrees of freedom (phononic, electronic, or magnetic), its derivative with respect to pressure p, the volume thermal expansion coefficient $\beta = -\frac{1}{V}(\frac{\partial S}{\partial p})_T$ is an extremely suitable quantity for studying different types of phase transitions. Over the last 10 years, the volume thermal expansion coefficient $\beta(T)$ has been established as an important tool for the analysis of quantum criticality. This can be explained as follows. If a system is dominated by a single energy scale $E^\star$ (e.g., the Fermi energy in a metal or the Debye energy if acoustic phonons dominate), the Grüneisen parameter $\Gamma = V_m/\kappa_T \cdot \beta(T)/C_p(T)$ [Ref. 1] is just given as the logarithmic derivative of the energy scale $E^\star$ with respect to pressure p [Refs. 2 and 3]

$$\Gamma(T) = \frac{1}{V_m \cdot E^\star}\frac{\partial E^\star}{\partial p}, \tag{1}$$

where $C_p(T)$ is the molar specific heat at constant pressure, and V_m is the molar volume. A diverging $\Gamma(T)$ can be expected when the relevant energy scale $E^\star$ vanishes, as it happens at a quantum critical point (QCP), i.e., a second order phase transition at $T = 0$. The quantity $\Gamma(T)$ thus offers a criterion for determining the existence of a QCP. In addition, the associated critical exponent can be used to distinguish between different classes of quantum phase transitions [Refs. 2 and 3]. A divergent $\Gamma(T)$ then implies that the specific heat $C_p(T)$ is less singular than the thermal expansion coefficient $\beta(T)$. As a consequence, the thermal expansion can be advocated to be the preferred quantity to investigate quantum critical phenomena. The theoretically expected diverging Grüneisen ratio has already been proven experimentally in the last decade with comprehensive and comparative high-resolution thermal expansion studies mainly on heavy fermion materials [Refs. 4–12]. These measurements required an extremely high sensitivity to detect a relative thermal length change of $\Delta L/L \approx 10^{-10}$ since by approaching absolute zero temperature, the thermal expansion coefficient $\beta(T)$ goes to zero, too.

The required resolution of $\Delta L = 10^{-2}$ Å for samples with a length $l \leq 5$ mm can only be achieved by capacitive dilatometry, first described by White in 1961 [Ref. 13]. White's design principles were adopted and improved by a number of researchers [Refs. 14–19]. Capacitance dilatometers based on parallel spring movement are well established and have been described for instance by Pott and Schefzyk [Ref. 15]. The major disadvantage of the dilatometers we used previously was the large size, which has been necessary to achieve the required high resolution. This represents a problem if one wants to investigate a QCP that is tuned by an external magnetic field. To determine the volume thermal expansion coefficient $\beta(T, H_c)$ of a single or polycrystal at the critical field H_c, it is necessary to measure the linear thermal expansion coefficient $\alpha(T)$ of one axis parallel $\Delta L(T)||H$ and of two axes perpendicular to the magnetic field $\Delta L(T)\perp H$. So far, magnetic field tuned QCPs cannot be studied with the highest possible resolution, since the large dilatometers cannot be rotated by 90° to adjust the sample perpendicular to the magnetic field. This motivated us to develop a much smaller dilatometer with the same extremely high resolution. Besides, we wanted to construct a cell, which could be used universally for thermal expansion and magnetostriction experiments. The magnetostriction $\Delta L(B)$, i.e., the length change of a sample induced by an applied magnetic field, is a thermodynamic quantity that provides important information about field induced phase transitions of matter at constant temperature and pressure. A miniaturized high resolution dilatometer could even be mounted on a rotator to study the angle dependence of quantum oscillations [Ref. 14] or the anisotropy of the order parameter of a superconductor.

Here, we introduce an extremely compact and miniaturized dilatometer constructed from a Be-Cu alloy using

electrical discharge machining. The resolution is determined by the diameter of the two capacitor plates and by the parallelism between them. The cells produced by the process described here are only marginally wider than the size of the capacitor plates. This optimized concept and the high level of manufacturing quality allows for an unprecedented resolution in a capacitive dilatometer of this compact size. Our dilatometer has a number of additional advantages. Due to the extremely small and compact design, we can achieve a good thermal homogeneity and an excellent temperature stabilization of the cell. This provides a faster thermal relaxation time and a high sensitivity of the cell on temperature changes and therefore makes the cells ideally suited even for high temperature measurements. Due to the extremely reduced cell size, an implementation in the widely used quantum design physical property measurement system (PPMS) could now be realized.

Our dilatometer has been operated successfully in a PPMS (2−300 K, and in magnetic fields up to 10 T), an exchange gas cryostat (3.5–300 K, and in fields up to 9 T), as well as in a dilution refrigerator with the dilatometer mounted in a vacuum (0.025–5 K in fields up to 20 T).

In Sec. II, we describe the design and manufacture of the dilatometer in detail. The thermometry and the capacitance measurement setup are discussed only briefly since we used standard methods. The measuring process as well as a room temperature test is described in Sec. III. The minimal force applied to the sample by the two leaf springs is determined in Sec. IV. In Sec. V, details of the cell operation and calibration, corrections due to the thermal expansion of the empty cell, and a thermal expansion test measurement of copper is presented. Finally, the extremely high resolution of our device is demonstrated by a measurement of a second order phase transition in a $YbNi_4P_2$ single crystal (Sec. V) and by quantum oscillations observed in the magnetostriction of bismuth (Sec. VI).

II. THE DILATOMETER

We first discuss the special requirements for the material of the dilatometer and afterwards introduce details of the design. Our goal is to manufacture a miniature capacitance dilatometer suitable for thermal expansion measurements in a broad temperature range from 300 K down to about 25 mK, as well as for magnetostriction experiments in fields up to at least 30 T. Therefore, we have to choose a material with high thermal conductivity, insensitivity to high magnetic fields, and well-known thermal expansion characteristics in the whole temperature range. The possible high-field applications also require a minimization of eddy currents in the metallic cell material, which are induced by time variation of the magnetic field ($dB/dt \neq 0$) and cause magnetic moments. The induced moments interact with the applied field and produce a torque on the movable part of the cell, resulting in an unintentional displacement of the capacitor plate. This effect depends on the rate dB/dt and gives rise to an irrepressible noise level. One main requirement concerning the cell material is to minimize this effect. In addition, to avoid mechanical stress during temperature sweeps, the cell material needs to be very homogeneous. Furthermore, thermal equilibrium in the cell material has to be reached fast. Finally, the material should be easy to machine, its magnetostrictive coefficient should be small, and it should not show any thermal or field induced phase transitions. The copper beryllium alloy with a beryllium concentration of 1.84% meets all criteria described above. Due to the low Be content, its thermal expansion and its thermal conductivity are nearly that of pure Cu, whereas its electrical conductivity is reduced by a factor of 30. Therefore, the influence of eddy currents induced by $dB/dt \neq 0$ is much smaller than in cells made from pure copper or silver.

The construction of our cell is based on the design of [Ref. 15] and is shown in Fig. 1. All parts (except some insulating spacers) are machined out of high-purity beryllium-copper. While the lower capacitor plate (6) is mounted to the fixed outer cell frame (3), the upper capacitor plate (5) is fixed to the movable part (1), which is held in the frame by two 30 μm thick BeCu leaf springs (2). In this parallelogram suspension, the upper plate can only move vertically [Ref. 20]. The sample is fixed by means of an adjustment screw (9) between the outer frame (3) and the movable part (1). In this construction, a length change of the sample (4) causes an equivalent displacement of the upper plate with respect to the lower, and therefore, a change in capacitance. The adjustment screw (9) contains a piston (10), which is hung up on the head of the screw. This prevents the warping of the sample during positioning. A 30° window between the movable part (1) and the fixed outer frame (3) allows for an easy mounting of the sample (4), but is small enough to ensure a good mechanical stability of the cell. Samples of less than 1 mm to 7 mm length can be measured. The two capacitor plates are separated by electrically insulating pieces of vespel (12) and 0.5 mm sapphire washers (11) and are surrounded by guard rings (7,8) to avoid stray electric fields. For both the lower (6) and the upper capacitor plate (5), three BeCu screws are used to fix the plates to the guard rings (7,8). In contrast to gluing the plates, this makes the construction much more stable and suitable for long term applications. Before mounting the dilatometer, the capacitor plates were polished within their frames. A uniform surface of the plates within their frames is necessary to achieve best parallel orientation of the plates. In its rest position, the capacitance of the dilatometer is about 5.4 pF, corresponding to a distance of 0.25 mm between the capacitor plates. After mounting the sample, the adjustment screw is used to reduce this distance to 0.067 mm, which corresponds to a capacitance of about 20 pF. By careful construction of the capacitance measuring circuit (shielding, avoiding of ground loops, etc.), the absolute value of the capacitance is measured with a resolution of 10^{-6} pF, which corresponds to a relative sensitivity $\Delta L/L \approx 10^{-10}$.

The original prototype design of [Ref. 15] was assembled from ten main parts, which determine the dimension of the cell. Our innovation is to produce the corpus of the cell, which originally consisted out of six different parts, from a single piece of BeCu, using milling and electrical discharge machining. The new main body (golden part of Fig. 1) now contains the whole movable part (1), both springs (2), as well as the middle part of the outer fixed cell frame (3). To include the springs in the main body, the BeCu block used for machining had to be annealed prior to processing for 3 h at 600 K.

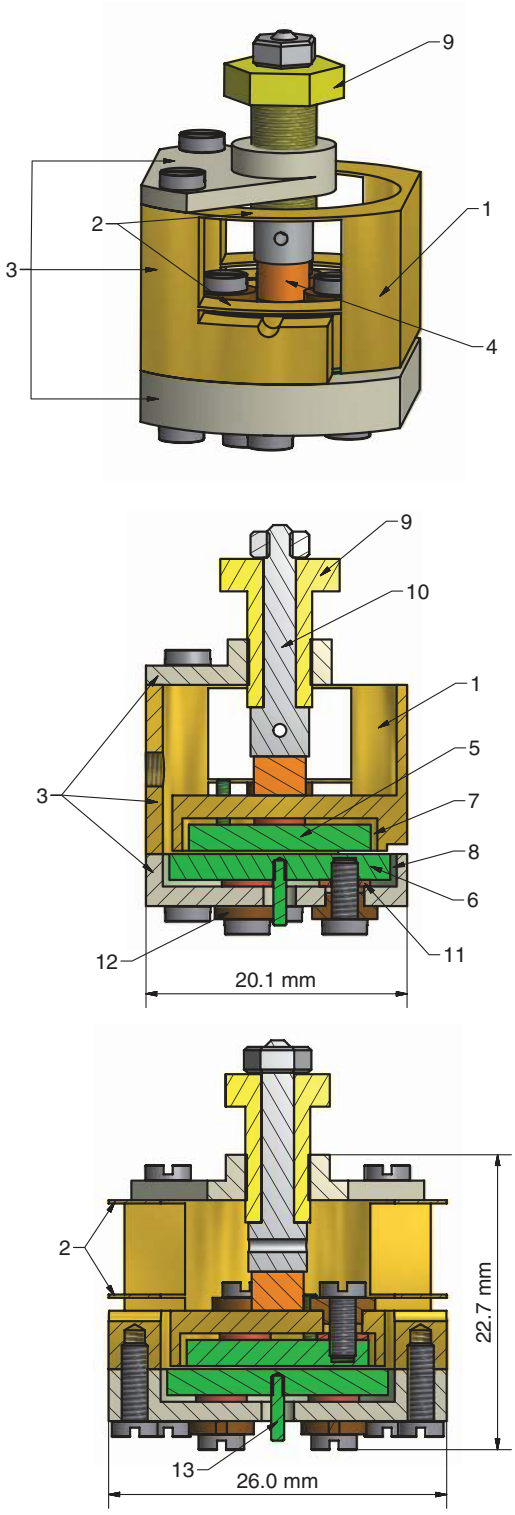

FIG. 1. A schematic view of the capacitive dilatometer. The upper panel shows a 3D-view, the middle panel, a side cut-away view, and the lower panel, a front cut-away view of the cell. (1) movable part, (2) Be-Cu flat springs, (3) fixed outer cell frame, (4) sample, (5) upper capacitor plate, (6) lower capacitor plate, (7) upper guard ring, (8) lower guard ring, (9) adjustment screw, (10) piston, (11) sapphire washer, (12) insulating piece of vespel, and (13) electrical connection.

This increases the hardness of the alloy by a factor of three and therefore enables the physical stability and elasticity of the springs, which are crucial for precisely plano-parallel vertical movement of the movable part with respect to the fixed outer cell frame. As shown in Fig. 1, the new manufacturing method makes it possible to extremely minimize the cell dimensions, which now allows the installation of the cell in extremely size limited sample chambers. Since our goal was to install the cell within an multi-functional insert of a commercial PPMS system and to rotate 360° within a inner vacuum chamber of 40 mm, it was particularly important to reduce the width of the dilatometer. Using the new production method, we achieved a width of only 20 mm with a cell diameter of 26 mm and an overall height of 22 mm. The new dilatometer has often great advantages compared to previous models. Although the whole mass of the cell could be reduced from more than 100 g to below 40 g, the full width of the capacitor plates and the resolution are completely preserved. Besides, due to the smaller cell mass and the significantly reduced numbers of contact surfaces, the thermal equilibrium in the cell material can be reached much faster upon cooling and heating. This makes the dilatometer suitable for measurements of thermal expansion at high temperature. Additionally, it is particularly suitable for magnetostrition measurements.

III. ROOM TEMPERATURE TEST

For an ideal plate capacitor with a surface area A and a plate distances d, the capacitance is given by

$$C = \epsilon_r \epsilon_0 A/d, \tag{2}$$

where $\epsilon_0 = 8.8542 \cdot 10^{-12} F/m$ is the electric field constant and ϵ_r is the dielectric constant of the medium in between the capacitor plates. We operate the dilatometer in vacuum ($\epsilon_r = 1$) or in Helium with pressure below 1 mBar ($\Delta\epsilon_r \leq 0.000000001$). For the room temperature test, we can assume $\epsilon_r = 1$, since the dielectric constant of air at atmospheric pressure is very close to unity ($\epsilon_r = 1.0006$). In our case, with circular shaped plates and a radius $r = 7$ mm of the smaller upper plate, we can determine the length change ΔL of the sample, i.e., the change in distance between the capacitor plates from the measured capacitance

$$\Delta L = \epsilon_0 \pi r^2 \frac{C - C_0}{C \cdot C_0}. \tag{3}$$

Here, C is the changing capacitance and C_0, the initial capacitance value.

The main source of errors in the measurement are slightly non-parallel capacitor plates [Refs. 15 and 21]. Due to the nonlinearity of Eq. (2), tilting of the plates always leads to an increase of the capacitance [Ref. 15]. A measure of the tilting is given by the capacitance C_{max}, which is the maximum capacitance just before the capacitor shorts. Taking into account the tilting of the plates, Pott and Schefzyk [Ref. 15] derived a corrected expression for the measured expansion ΔL

$$\Delta L = \epsilon_0 \pi r^2 \frac{C - C_0}{C \cdot C_0} \left(1 - \frac{C \cdot C_0}{C_{max}^2}\right). \tag{4}$$

We use Eq. (4) to test the functionality of the dilatometer at room temperature. Figure 2 shows a photo of the

FIG. 2. Test setup for our dilatometer with a standard dial gauge. The sensors tip of the dial gauge is set perpendicular to the upper surface of the movable part.

setup, where a standard dial gauge with a resolution of 1/100 mm is used as a reference to measure the length change. First, the sensor tip of the dial gauge is set perpendicular to the upper surface of the movable part. When the adjustment screw is tightened, the dial gauge indicates the vertical movement of the movable part, including the upper capacitor plate. The change of capacitance is simultaneously measured by a commercial capacitance bridge [Ref. 22]. Figure 3 compares the measured length change to calculated values based on different short-circuit capacitances C_{max}. The experimental values are in very good agreement with the calculated values for $C_{max} = 150$ pF. The short-circuit capacitance can also be approximated by carefully decreasing the plate distance with the adjustment screw until the capacitor shorts. The last and highest value measured gives C_{max}. The value obtained by this method is $C_{max} = 145$ pF, which agrees with the calculated value of

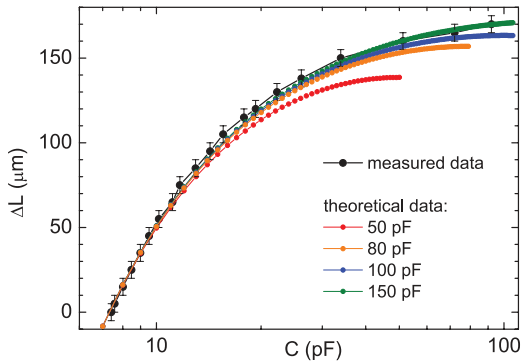

FIG. 3. Comparison of the measured data to calculated values based on formula (4) for different short-circuit capacities.

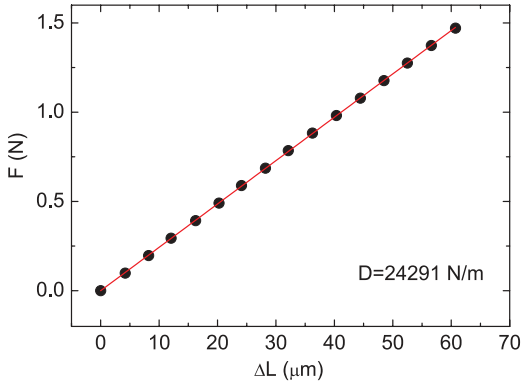

FIG. 4. Measurement of the spring force by placing weights on top of the movable part.

150 pF. Disassembling and reassembling the dilatometer did not significantly affect the value of C_{max}. The different dilatometers tested have a short-circuit capacitance between 130 and 230 pF. From Eq. (3), the sensitivity is proportional to $C^2 \approx C \cdot C_0$. However, the contribution from errors caused by the tilted capacitor plates increases with increasing C as well. A good compromise is a measuring capacitance between 20 and 25 pF, which yields for the cell with $C_{max} = 150$ pF an absolute error between 1.7% and 2.7%.

IV. SPRING FORCE EXERTED ON THE SAMPLE

A small spring force exerted on the sample by the two leaf springs is inevitable with the described design. This is important, since the induced pressure could lead to changed sample properties. To estimate the magnitude of the spring force, we measured the spring constant at room temperature. For this purpose, the movable part of the cell was weighed down stepwise with weights up to 150 g. The resulting length change ΔL was calculated from the measured capacitance using Eq. (3). Figure 4 shows the obtained linear relation between the length change and the applied force, from which we derived a force constant $D = 24\,291$ Nm^{-1}. Since the modulus of elasticity of copper alloys remains almost constant from room temperature to below 1 K, this value is applicable to the whole temperature range of operation. Figure 5 shows the relation between the nominal capacitance and the plate distance, and the resulting force for the obtained spring constant. Since

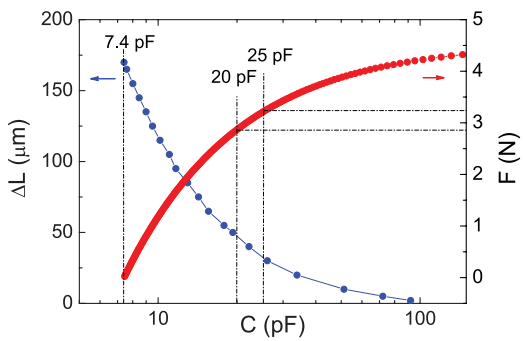

FIG. 5. Resulting spring force exerted on sample at common working capacitances in between 20–25 pF.

FIG. 6. Left: The complete measuring probe with gold plated thermal anchors and connectors for capacitance and temperature measurements. Right: Dilatometer within the multi-functional chamber. The position of the thermometer is highlighted by the white frame.

the dilatometer is operated between 20 and 25 pF, which corresponds to a plate distance of 50–35 μm, one obtains a spring force of 3 N. In most measurements, such a weak force can be neglected.

V. THERMAL EXPANSION BETWEEN $T = 5$ K AND $T = 300$ K

We performed thermal expansion measurements in a PPMS in the temperature range between 5 and 300 K. The sample space was kept under a helium atmosphere with typically 1 mbar of helium pressure, which ensures a good thermal stability of the cell and the included sample. Figure 6 shows the dilatometer mounted within a PPMS multi-functional insert. The two capacitor plates are connected by coaxial cables to the measuring bridge. To avoid ground loops, the cell is insulated from the rest of the insert by a coaxial cable feed-through made of plastic. The multi-functional PPMS insert is thermally coupled to the annular region at the bottom, where heaters warm the helium gas to the correct temperature, via a pin connector. Gold plated thermal anchors mounted on a copper block just above the cell touch the inner chamber of the PPMS cooling channels and further improve the thermal coupling of the cell. Additional anchors are mounted above the insert at several points of the measurement probe to reduce the temperature successively from the top of the cryostat down to the cell. To reduce the heat leak caused by the coaxial cables, they are wrapped around the measurement probe. The temperature is measured by a Cernox resistance thermometer enclosed in the head of the cell, near the sample (see white frame in Fig. 6).

A. Calibration of the cell background and test measurement of silver

The use of different materials in the dilatometer assembly leads to a temperature-dependent background due to different thermal expansion coefficients. We minimized this effect in our cell design, where nearly all components are machined from Be-Cu alloy. The only exceptions are sapphire washers and electrically insulating parts made of vespel (see Fig. 1). In the following, the remaining cell background is calibrated by a reference measurement of a copper sample. To further test this calibration, we measure the thermal expansion of silver and compare the results to literature values.

In a thermal expansion experiment, both the sample length and the length of the dilatometer cell itself vary with temperature. The measured length change of the sample ΔL_{meas}^{sample} is the difference between the actual length change ΔL^{sample} of the sample and the length change of the cell ΔL^{cell}

$$\Delta L_{meas}^{sample} = \Delta L^{sample} - \Delta L^{cell}. \tag{5}$$

To calibrate the cell effect ΔL^{cell}, we measure the thermal expansion of a reference sample with a thermal expansion coefficient close to that of the cell body material $Cu_{1-x}Be_x$. Since the beryllium content $x = 1.84$ is very low, we can use high-purity copper (99.999%) as a reference, where the thermal expansion in the relevant temperature range is well known from literature [Ref. 23]. This experiment measures the empty cell effect, i.e., the deviation of the cell length change ΔL^{cell} from the literature values ΔL_{lit}^{Cu} for a sample of pure copper

$$\Delta L_{meas}^{Cu} = \Delta L^{empty\ cell} = \Delta L_{lit}^{Cu} - \Delta L^{cell}. \tag{6}$$

The cell effect ΔL^{cell} is therefore the difference of the length change of the copper sample and the empty cell effect

$$\Delta L^{cell} = \Delta L_{lit}^{Cu} - \Delta L^{empty\ cell}. \tag{7}$$

The cell effect results mainly from the fact that by measuring a sample with a length L_0 a respective part of the BeCu-cell of the same length is missing. Figure 7 shows the measured empty cell effect (black), the thermal expansion of copper (red), and the resulting total cell effect (blue), normalized to the sample length of 4 mm. The empty cell effect is quite small, the thermal expansion of the cell deviates only slightly from that of a block of pure copper, demonstrating the high quality of the cell.

To obtain the true length change of a sample measured with this dilatometer, the calibrated cell effect is added to the

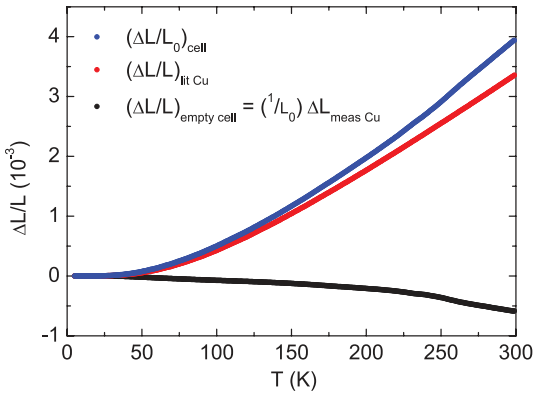

FIG. 7. Measured empty cell effect (black), literature values for the relative length change of copper (red), and calculated cell effect (blue).

measured length change ΔL_{meas}^{sample}

$$\Delta L^{sample} = \Delta L_{meas}^{sample} + \Delta L^{cell},$$
$$= \Delta L_{meas}^{sample} - \Delta L^{empty\ cell} + \Delta L_{lit}^{Cu}. \quad (8)$$

The relative length change of the sample normalized to its room temperature length L_0 is therefore given by

$$\left(\frac{\Delta L}{L_0}\right)^{sample} = \frac{\Delta L_{meas}^{sample} - \Delta L^{empty\ cell}}{L_0} + \left(\frac{\Delta L}{L}\right)_{lit}^{Cu}, \quad (9)$$

where the last term represents the literature value for the relative thermal expansion of pure copper, which is independent of the sample length.

To test the calibration of the cell effect and the sensitivity of the dilatometer, we performed an additional measurement of a silver sample (purity 99.999%, $l_0 = 4$ mm, 3 mm diam.). The results for the relative length change and the thermal expansion coefficient are shown in Fig. 8, where they are compared to literature values ([Refs. 24 and 25]). The inset shows the relative error estimated from a comparison to tabulated literature data. We observe a very good agreement in the whole temperature range. In the high-temperature region ($T \geq 25$ K), the relative error is smaller than 3% but seems to become quite large (up to 17%) at low temperatures ($T \leq 25$ K). This relative error appears quite high, however the thermal expansion coefficient of silver in this temperature range is extremely small ($\leq 2 \times 10^{-6}\mathrm{K}^{-1}$) and also becomes dependent of both sample purity and preparation. Therefore, the absolute error values are still several orders of magnitude lower than the thermal expansion coefficient expected in most materials.

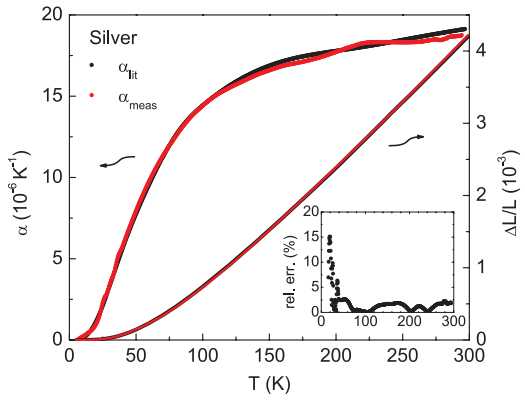

FIG. 8. Relative length change $\Delta l/l$ and thermal expansion coefficient $\alpha(T)$ of silver as a function of temperature ($5 \leq T \leq 300$ K). The inset shows the relative error estimated from a comparison with literature data [Ref. 23].

The thermal expansion coefficient $\alpha(T)$ shows an unexpected temperature dependence, with a broad peak between 215 and 240 K. Since this anomaly is observed repeatedly in measurements of different samples, it must be associated to the cell material itself. One possible reason could be the unavoidable oxidation of the BeCu-frame. Reference 26 shows that CuO exhibits two phase transitions in the same temperature region: one second order phase transition from a paramagnetic to an incommensurate antiferromagnetic state at a temperature $T_{high} = 230$ K, and a first order phase transition to the commensurate antiferromagnetic state at $T_{low} = 213$ K. Unfortunately, we cannot exactly determine, which one of the two transitions is observed. Since the transition is not exactly reproducible for every measurement, it cannot be entirely corrected by the calibration measurement. As one can see in Fig. 8 on the thermal expansion coefficient of silver, the anomaly still influences the measurement after the cell effect has been corrected. Therefore, a precise determination of the thermal expansion coefficient in the temperature range $215 \leq T \leq 240$ K is not possible. Nevertheless, since the observed effect is characterized by a broad peak, clear anomalies should still be detectible, even in this temperature range. For the next cell generation, we plan on coating the cells in gold immediately after production. This way we hope to at least lower the influence of the anomalies.

B. Thermal expansion at millikelvin temperatures

To give an impression of the sensitivity of our dilatometer, we show the relative length change and the low-temperature thermal expansion coefficient of an $YbNi_4P_2$ single crystal with a length of $l = 1$ mm, which is a ferromagnet below $T_C = 0.15$ K (see Fig. 9, [Ref. 27]). Here, the cell is mounted on a cold finger of a dilution refrigerator. A

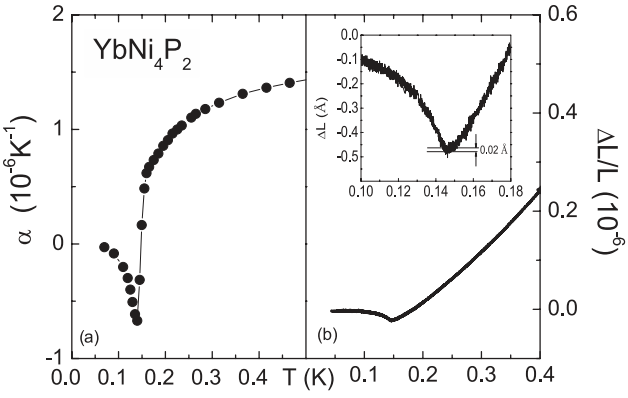

FIG. 9. Low-temperature thermal expansion coefficient $\alpha(T)$ (a) and relative length change $\Delta L/L_0(T)$ (b) of an $YbNi_4P_2$ single crystal, measured parallel to the c-axis. The sharp λ-type anomaly at T_C (a) of the second order phase transition demonstrates the high sensitivity of our dilatometer and the very good quality of the sample. The inset shows the high resolution of 0.02 Å at low temperatures.

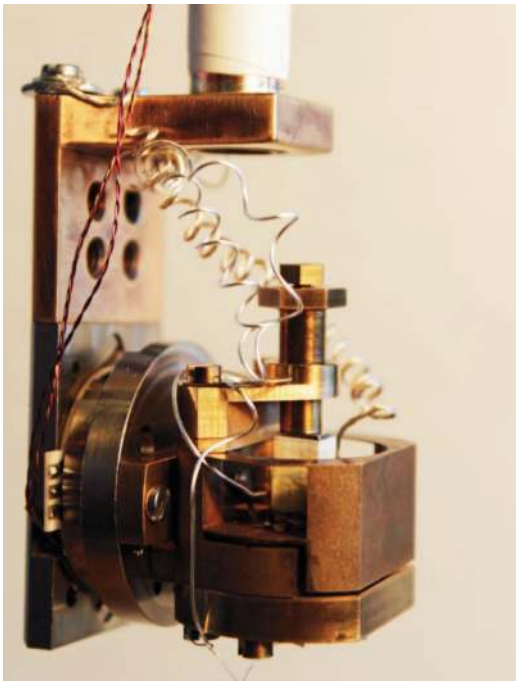

FIG. 10. Photograph of the cell mounted on a Attocube rotator.

sharp λ-type anomaly observed in $\alpha(T)$ at T_C indicates the second-order phase transition. The width of this anomaly is only about 20 mK, which is also observed in the specific heat. It demonstrates that, due to the tiny cell size, thermal equilibrium for both the cell and the sample is reached very quickly and a complicated setup, where the sample is thermally isolated from the cell, is not necessary. The inset shows the extraordinary sensitivity of our dilatometer with a very high resolution of 0.02 Å.

VI. MAGNETOSTRICTION MEASUREMENTS

The dilatometer has also been designed for the use in magnetic field as high as 30 T. Due to its small size, it can be mounted on a rotator and still fits inside the inner vacuum chamber (40 mm diameter) of a dilution refrigerator. Figure 10 shows a photograph of the setup. The dilatometer can be rotated around a horizontal rotation axis using a piezoelectric rotator provided by Attocube Systems. The one-axis rotation set-up allows a rotation of 360°. The rotator is made of non-magnetic materials, which allow the operation in very strong magnetic fields (current max. tested field: 31 T). The rotator angle is measured by a rotary potentiometer with an accuracy of about 0.05°.

We first measured the B-field dependence of the cell effect at various angles. For very weakly paramagnetic metal like copper, one expects a small quadratic magnetostriction, which is in good agreement with the data shown in Fig. 11. The B-field dependence at the empty cell effect $\Delta L(B)$ follows a power law with an exponent close to two: $\Delta L(B) = 5.2 \times 10^{-9}$ cm $\times$ $(B[\mathrm{T}])^{1.8}$. This B-field dependence of the empty cell is very small, making the cell a good choice for dilatometers designed for magnetostriction measurements. A 90° rotation of the cell around the horizontal rotation axis does not significantly change the B-field dependent background. Eddy currents cause additional heating of the cell, depending on the field sweep rate. At a typical rate of 0.01 T/min, we observed at a base temperature of $T = 25$ mK a slight warming up of about 2–3 mK.

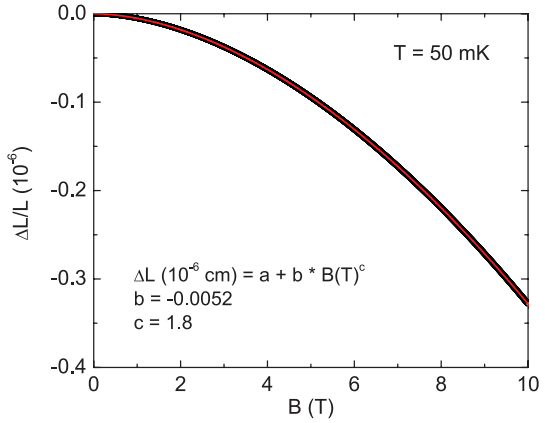

FIG. 11. Empty cell effect as a function of the magnetic field: $\Delta L(B) = 5.2 \times 10^{-9}$ cm $\times$ $(B[\mathrm{T}])^{1.8}$.

To give an example of the exceptional sensitivity of our miniature dilatometer, we show measurements of the quantum oscillations in the magnetostriction of bismuth. Figure 12 shows the magnetostriction measured at 0.025 and 4.2 K along the high-symmetry crystalline axis for fields up to 10 T. At low temperature, the oscillatory phenomena, driven by the de Haas-van Alphen effect becomes clearly visible at magnetic fields as small as 0.2 T. In the field range ≤ 2 T, more than 20 full periods were identified (see the inset of Fig. 12). The de Haas-van Alphen period was found to be 0.15 T^{-1}, in good agreement with the results obtained from other methods [Refs. 28 and 29]. This period corresponds to the maximum cross section of the hole ellipsoid of the Fermi surface. Due to the great sensitivity of the new dilatometer, displacements as small as 0.02 Å have been resolved.

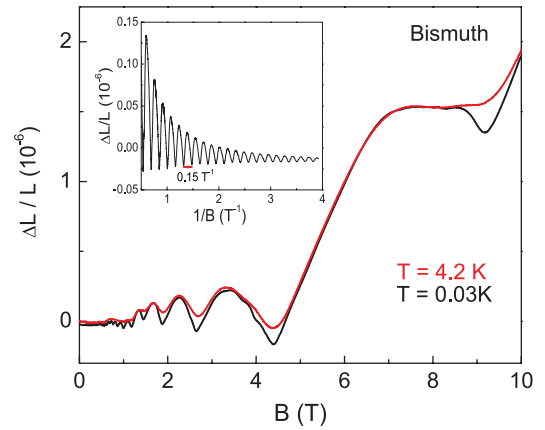

FIG. 12. Quantum oscillations of the magnetostriction for a field along trigonal at $T = 0.03$ and 4.2 K. Inset: Low-field oscillatory magnetostriction at 0.03 K, up to 2 T.

VII. CONCLUSION

We reported on the design, construction, and calibration of a miniaturized capacitance dilatometer for thermal expansion and magnetostriction measurements. The most important novelty of our work was to reduce the cell dimensions enough to integrate the dilatometer into commercial measurement systems like the PPMS by quantum design. Due to the very small probe space available and thermal stability issues, no thermal expansion and magnetostriction insert with a comparable sensitivity of $\Delta L/L = 10^{-10}$ have yet been developed for these common laboratory setups. Our innovative production method allows us to minimize the overall frame size of the cell without reducing the sample space or the diameter of the capacitor plates by the same amount, which preserves an extremely high sensitivity. Furthermore, the space saving design of the cell body leaves enough room for an integrated thermometer, so that the sample temperature can be monitored very precisely. This ensures an easy calibration and a very good reproducibility of the results obtained with our measurement setup. Besides, due to the dilatometer small size, it can be mounted on a rotator and still fits inside the inner vacuum chamber of a dilution refrigerator. The one-axis rotation set-up allows a rotation of 360°.

ACKNOWLEDGMENTS

We are especially thankful to P. Gegenwart for his assistance and encouragement during the early stages of this project and together with C. Stingl for their continued interest and assistance. We are also indebted to T. Lühmann, who continuously improved software needed to run the experiments. Appreciation is given to the mechanicians of our workshop, J. Faltin, T. Thomas, and J. Scharsach, who have manufactured all the precise parts of the dilatometer. We also thank C. Klausnitzer for the help with technical drawings, and L. Steinke for valuable comments on the manuscript. This work has been supported by the DFG Research Unit 960 (Quantum Phase Transitions).

[1] E. Grüneisen, Ann. Phys. (Leipzig) **39**, 257 (1912).
[2] L. Zhu, M. Garst, A. Rosch, and Q. Si, Phys. Rev. Lett. **91**, 066404 (2003).
[3] M. Garst, Ph.D. dissertation, TH Karlsruhe, 2003.
[4] R. Küchler, N. Oeschler, P. Gegenwart, T. Cichorek, K. Neumaier, O. Tegus, C. Geibel, J. Mydosh, F. Steglich, L. Zhu, and Q. Si, Phys. Rev. Lett. **91**, 066405 (2003).
[5] R. Küchler, P. Gegenwart, K. Heuser, E. W. Scheidt, G. R. Stewart, and F. Steglich, Phys. Rev. Lett. **93**, 096402 (2004).
[6] R. Küchler, P. Gegenwart, J. Custers, O. Stockert, N. Caroca-Canales, C. Geibel, J. Sereni, and F. Steglich, Phys. Rev. Lett. **96**, 256403 (2006).
[7] G. Donath *et al.*, Phys. Rev. Lett. **100**, 136401 (2008).
[8] T. Westerkamp *et al.*, Phys. Rev. Lett. **102**, 206404 (2009).
[9] N. T. Huy and A. de Visser, Phys. Rev. B **75**, 212405 (2007).
[10] A. de Visser *et al.*, Physica B **163**, 49–52 (1990).
[11] T. Lorenz *et al.*, Phys. Rev. Lett. **100**, 067208 (2008).
[12] F. Weickert *et al.*, Phys. Rev. B **85**, 184408 (2012).
[13] G. K. White, Cryogenics **1**, 151 (1961).
[14] G. Brändli and R. Griessen, Cryogenics **13**, 299 (1973).
[15] R. Pott and R. Schefzyk, J. Phys. E: Sci. Instrum. **16**, 4456 (1983).
[16] M. Rotter, H. Müller, E. Gratz, M. Doerr, and M. Loewenhaupt, Rev. Sci. Instrum. **69**, 2742 (1998).
[17] G. M. Schmiedeshoff *et al.*, Rev. Sci. Instrum. **77**, 123907 (2006).
[18] J. J. Neumeier, R. K. Bollinger, G. E. Timmins, C. R. Lane, R. D. Krogstad, and J. Macaluso, Rev. Sci. Instrum. **79**, 033903 (2008).
[19] J. H. Park *et al.*, Rev. Sci. Instrum. **80**, 116101 (2009).
[20] M. O. Steinitz, J. Genossar, W. Schnepf, and D. A. Tindall, Rev. Sci. Instrum. **57**, 297 (1986).
[21] J. Genossar and M. O. Steinitz, Rev. Sci. Instrum. **61**, 2469 (1990).
[22] M. O. Steinitz, Phys. Can. **62**(2), 99 (2006).
[23] F. R. Kroeger and C. A. Swenson, J. Appl. Phys. **48**, 853–864 (1977).
[24] G. White and J. G. Collins, J. Low Temp. Phys. **7**, 43–75 (1972).
[25] G. White and M. Minges, Int. J. Thermodyn. **18**, 1269–1327 (1997).
[26] X. G. Zheng *et al.*, Philos. Mag. Lett. **79**, 819 (1999).
[27] C. Krellner *et al.*, New J. Phys. **13**, 103014 (2011).
[28] K. Behnia, L. Balicas, and Y. Kopelevich, Science **317**, 1729 (2007).
[29] L. Li *et al.*, Science **321**, 547 (2008).